

Compressive time-lapse seismic monitoring of carbon storage and sequestration with the joint recovery model

Ziyi Yin¹, Mathias Louboutin², Felix J. Herrmann^{1,2}

¹ School of Computational Science and Engineering, Georgia Institute of Technology

² School of Earth and Atmospheric Sciences, Georgia Institute of Technology

SUMMARY

Time-lapse seismic monitoring of carbon storage and sequestration is often challenging because the time-lapse signature of the growth of CO₂ plumes is weak in amplitude and therefore difficult to detect seismically. This situation is compounded by the fact that the surveys are often coarsely sampled and not replicated to reduce costs. As a result, images obtained for different vintages (baseline and monitor surveys) often contain artifacts that may be attributed wrongly to time-lapse changes. To address these issues, we propose to invert the baseline and monitor surveys jointly. By using the joint recovery model, we exploit information shared between multiple time-lapse surveys. Contrary to other time-lapse methods, our approach does not rely on replicating the surveys to detect time-lapse changes. To illustrate this advantage, we present a numerical sensitivity study where CO₂ is injected in a realistic synthetic model. This model is representative of the geology in the southeast of the North Sea, an area currently considered for carbon sequestration. Our example demonstrates that the joint recovery model improves the quality of time-lapse images allowing us to monitor the CO₂ plume seismically.

INTRODUCTION

Time-lapse seismic imaging technology has recently been deployed by Carbon Capture and Storage (CCS) practitioners to monitor CO₂ dynamics in porous media over long periods of time, with the Sleipner project in Norway as a pioneer (Arts et al., 2003; Furre et al., 2017). There have been several major developments to adapt compressive sensing (Janiszewski et al., 2014; Herrmann and Hennenfent, 2008) and machine learning (Bharadwaj et al., 2020; Kaur et al., 2020) to improve the productivity of (time-lapse) seismic data acquisition (Oghenekohwo et al., 2017; Wason et al., 2017) and imaging (Oghenekohwo and Herrmann, 2015) by exploiting similarities between baseline and monitor surveys. Recent work by Li et al. (2020) indicates the potential benefits of a coupled-physics framework where the slow-time subsurface CO₂ flow, a rock physics model, and the fast-time wave physics are combined to better understand the dynamics of CO₂ plumes and their effect on time-lapse seismic data for the duration of a CCS project. Because the time-lapse signal of CO₂ plumes is weak, it continues to pose challenges on the robustness of time-lapse imaging (Lumley et al., 1997).

To address some of these challenges, Oghenekohwo et al. (2017); Wason et al. (2017) proposed the joint recovery model (JRM) designed to reap the benefits of low-cost randomized non-replicated acquisition. It takes advantage of the fact that time-lapse seismic data and subsurface structure undergoing localized changes share information among the different vintages. In this extended abstract, we present a synthetic

case study to make the case that the dynamics of CO₂ plumes can indeed be monitored with active-source surface seismic. The presented work can be considered as a continuation of recent contributions by Li et al. (2020), who considered seismic monitoring in a much simpler geological setting involving cross-well tomography. In our study, we consider a 2D subsection of the BG Compass model with a geology representative of the southeast of the North Sea. Blunt sandstones in this area are considered as possible reservoirs for injection of CO₂. Aside from assessing the sensitivity of seismic imaging towards monitoring CO₂ plumes, we also study the effects of changes in the acquisition and the presence of noise, and how the JRM can be deployed to mitigate these effects of incomplete and non-replicated data.

Our contributions are organized as follows. First, we briefly discuss full-waveform inversion and its linearization as part of time-lapse seismic imaging. Next, we introduce our joint inversion framework that explores commonalities between seismic images associated with the different vintages collected for the duration of a CCS project. We conclude by discussing a realistic time-lapse imaging experiment juxtaposing images obtained by inverting the vintages independently or jointly with JRM.

METHODOLOGY

We first briefly introduce the theoretical framework on which our wave-equation based monitoring framework for CCS is based. While we understand that more complex wave physics, e.g. elastic (Thomsen, 1986) and nonlinear inversions (Li et al., 2012), may eventually be needed, we begin by deriving a model based on the scalar wave equation parameterized by the squared slowness. We start by introducing the objective for full-waveform inversion and its linearization with respect to an assumed given smooth background model. Based on this linearization, we propose a joint recovery model, which we solve computationally efficiently with linearized Bregman iterations (Yin et al., 2008; Witte et al., 2019b).

Full-waveform inversion (FWI) and its linearization

To derive a joint wave-based seismic monitoring system, we start by introducing the objective of full-waveform inversion for the baseline ($j = 1$) and multiple monitor surveys ($2 \leq j \leq n_v$) with $n_v \geq 2$ as the number of vintages. For each vintage, this data misfit objective reads

$$\min_{\mathbf{m}_j} \|\mathbf{d}_j - \mathcal{F}_j(\mathbf{m}_j)\|_2^2 \quad \text{for } j = \{1, 2, \dots, n_v\}. \quad (1)$$

In this expression, \mathcal{F}_j is the nonlinear forward modeling operator, which for given sources generates synthetic data at the receiver locations from the discretized time-lapse model parameters \mathbf{m}_j . The observed data is, for each vintage, collected in the vector \mathbf{d}_j . When provided with background velocity models

$\bar{\mathbf{m}}_j$ for each vintage, the above forward model can be linearized yielding

$$\min_{\delta \mathbf{m}_j} \|\delta \mathbf{d}_j - \nabla \mathcal{F}_j(\bar{\mathbf{m}}_j) \delta \mathbf{m}_j\|_2^2, \quad (2)$$

where $\delta \mathbf{d}_j = \mathbf{d}_j - \mathcal{F}_j(\bar{\mathbf{m}}_j)$ are the linearized datasets for each vintage and $\nabla \mathcal{F}_j$ the linearized forward operator relating perturbations in the squared slowness for each vintage, $\delta \mathbf{m}_j$, to linearized data $\delta \mathbf{d}_j$.

Time-lapse monitoring with the joint recovery model

There exists an extensive literature on wave-based time-lapse imaging aimed at producing images that show time-lapse differences in the image space by carrying out inversion rather than imaging (Qu and Verschuur, 2017; Yang et al., 2016; Quei ber and Singh, 2013; Maharramov et al., 2019). A prominent example of such inversion method is formed by time-lapse monitoring via double differences (Zhang and Huang, 2013; Yang et al., 2015) where differences are obtained by inverting differences between the monitor and baseline residuals rather than between observed and synthetic monitoring data. While this type of approach can lead to good results, it assumes the baseline and monitor surveys to be relatively noise free, well sampled, and above all replicated—i.e. the acquisition geometries between different surveys need to be identical.

In our approach, we build on a low-cost formulation for time-lapse seismic monitoring designed to handle low-cost non-replicated sparsely sampled surveys. The basic idea of this approach is to focus on what is shared amongst the different vintages rather than focusing on what is different. We argue that time-lapse monitoring benefits from such an approach if the Earth model being monitored undergoes relatively localized changes, an assumption that likely holds during CCS. To arrive at a successful joint inversion scheme, we augment the block diagonal linear system undergirding independent imaging (by minimizing Equation 2 independently for each vintage) with an extra column and a corresponding unknown common component. With these steps, we write

$$\mathbf{A} = \begin{bmatrix} \frac{1}{\gamma} \nabla \mathcal{F}_1(\bar{\mathbf{m}}_1) & \nabla \mathcal{F}_1(\bar{\mathbf{m}}_1) & \mathbf{0} & \mathbf{0} \\ \dots & \mathbf{0} & \dots & \mathbf{0} \\ \frac{1}{\gamma} \nabla \mathcal{F}_{n_v}(\bar{\mathbf{m}}_{n_v}) & \mathbf{0} & \mathbf{0} & \nabla \mathcal{F}_{n_v}(\bar{\mathbf{m}}_{n_v}) \end{bmatrix}. \quad (3)$$

This matrix \mathbf{A} relates the linearized data for each vintage $\{\delta \mathbf{d}_j\}_{j=1}^{n_v}$, collected in the vector $\mathbf{b} = [\delta \mathbf{d}_1^\top, \dots, \delta \mathbf{d}_{n_v}^\top]^\top$, to the common component \mathbf{z}_0 and innovations with respect to this common component $\{\mathbf{z}_j\}_{j=1}^{n_v}$ all collected in the vector $\mathbf{z} = [\mathbf{z}_0^\top, \dots, \mathbf{z}_{n_v}^\top]^\top$. This formulation emphasizes what is common amongst the vintages when γ is close to 0, given that $0 < \gamma < n_v$ is generally a good choice in practice (Li, 2015).

In JRM, surveys for all vintages are explicitly related to the common component. Therefore, when acquisition geometries for different surveys are not replicated, this joint formulation recovers the common component better because the different surveys collect complementary information through the different acquisitions. As a result of the improved recovery of the common component, we can also expect the images for the different vintages themselves to be better recovered. This behavior has indeed been confirmed by several numerical experiments (Oghenekohwo and Herrmann, 2017; Wason et al.,

2015; Oghenekohwo and Herrmann, 2015) and in the presence of noise as reported by Chevron (Wei et al., 2018; Tian et al., 2018).

Time-lapse monitoring with linearized Bregman

The above joint recovery model reaps the benefit of randomized seismic acquisition with techniques adapted from Compressive Sensing, where subsampling related interferences (e.g. aliases or simultaneous source cross talk) are rendered into incoherent noise (Herrmann and Hennenfent, 2008; Herrmann, 2010). As shown by Yang et al. (2020); Witte et al. (2019b), these incoherent artifacts can be mapped back to coherent energy by solving the following minimization problem:

$$\begin{aligned} \min_{\mathbf{x}} \quad & \lambda \|\mathbf{C}\mathbf{x}\|_1 + \frac{1}{2} \|\mathbf{C}\mathbf{x}\|_2^2 \\ \text{subject to} \quad & \|\mathbf{b} - \mathbf{A}\mathbf{x}\|_2 \leq \sigma \end{aligned} \quad (4)$$

with \mathbf{C} the forward curvelet transform, λ a threshold parameter, and σ the magnitude of the noise. The advantage of this strictly convex formulation is that it can be solved via linearized Bregman iterations that for $\sigma = 0$ correspond to doing iterative soft thresholding on the dual variable—i.e., we carry out the following update at iteration k

$$\begin{aligned} \mathbf{u}_{k+1} &= \mathbf{u}_k - t_k \mathbf{A}_k^\top (\mathbf{A}_k \mathbf{x}_k - \mathbf{b}_k) \\ \mathbf{x}_{k+1} &= \mathbf{C}^\top S_\lambda (\mathbf{C} \mathbf{u}_{k+1}), \end{aligned} \quad (5)$$

where \mathbf{A}_k represents the matrix in Equation 3 for a subset of shots randomly selected from sources in each vintage. The vector \mathbf{b}_k contains the extracted shot records from \mathbf{b} and the symbol $^\top$ refers to the adjoint. Sparsity is promoted via curvelet-domain soft thresholding $S_\lambda(\cdot) = \max(|\cdot| - \lambda, 0) \text{sign}(\cdot)$ with λ as the threshold.

Compared to other ℓ_1 -norm solvers, linearized Bregman iterations are relatively simple to implement and have shown to work well in the context of least-squares imaging (Yang et al., 2020; Witte et al., 2019b) as long as the steplength t_k and threshold λ are appropriately chosen. A general choice of dynamic steplength t_k is given by $t_k = \|\mathbf{A}_k \mathbf{x}_k - \mathbf{b}_k\|_2^2 / \|\mathbf{A}_k^\top (\mathbf{A}_k \mathbf{x}_k - \mathbf{b}_k)\|_2^2$ (Lorenz et al., 2014) and the threshold λ is typically chosen to be proportional to the maximum of $|\mathbf{u}_k|$ in the first iteration ($k = 1$). After solving problem 4 by the iterative process 5, estimates for the baseline and monitor images are obtained via $\widehat{\delta \mathbf{m}}_j = \widehat{\mathbf{x}}_0 + \widehat{\mathbf{x}}_j$, $j = 1, 2, \dots, n_v$ where $\widehat{\mathbf{x}}$ minimizes problem 4.

NUMERICAL CASE STUDY BLUNT SANDSTONE SW NORTH SEA

By means of a realistic synthetic experiment, we demonstrate deployment of the joint recovery model to monitor CCS. To create a realistic monitoring scenario, we start by modeling the development of a CO2 plume with a numerical scheme that solves the two-phase flow equation. Next, we translate the CO2 concentration to time-lapse changes in acoustic wavespeed perturbations, which we use to generate seismic data for the vintages. These datasets, collected with different acquisitions, serve as input to our imaging scheme.

Geologic and rock physical setting

To numerically validate the potential improvement of time-lapse monitoring via our joint recovery model, we consider

the 2D 2×15.9 km subset of the BG Compass model plotted in Figure 1. This figure contains a plot of the spatial distribution for the permeability and is representative for CCS in Blunt sandstones. Following the stratigraphy in the real setting, the synthetic stratigraphic section in Figure 1 can roughly be divided into three main sections, namely (i) the highly porous (average 22%) and permeable (> 170 mD) Bunter Sandstone of about 300 – 500m thick and that serves as the CO₂ reservoir (red area in Figure 1, which includes location of the injection well, denoted by the white \times , and the production well denoted by the yellow \bullet); (ii) the primary seal (permeability $10^{-4} - 10^{-2}$ mD) made of the Rot Halite Member, which is 50m thick and is typically continuous (black layer in Figure 1); (iii) the secondary seal made of the Haisborough group, which is > 300 m thick and consists of low-permeable (permeability 15 – 18mD) mudstones.

By assuming a linear relationship between the compressional wavespeed and permeability in each stratigraphic section, we arrive at the synthetic permeability model plotted in Figure 1. To convert wavespeed to permeability, we assume for each section that an increase of 1km/s in the compressional wavespeed corresponds to an increase of 1.63mD in the permeability. Given these values for the permeability, we derive values for the porosity using the Kozeny-Carman equation (Costa, 2006)

$$K = \phi^3 \left(\frac{1.527}{0.0314 * (1 - \phi)} \right)^2$$

where K and ϕ denote permeability (mD) and porosity (%) with constants taken from the Strategic UK CCS Storage Appraisal Project report.

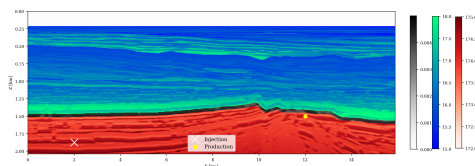


Figure 1: Permeability of 2D slice of BG Compass model including injection (white \times) and production well (yellow \bullet).

Simulation of CO₂ dynamics

We use the open-source software [FwiFlow](#) (Li et al., 2020) to numerically simulate the growth of the CO₂ plume by solving the partial differential equations for two-phase flow for a period of 60 years with a time step of 20 days and a grid spacing of 25m. While our numerical simulations are in 2D, we assume the permeability model to extend by 1.6 km in the third (perpendicular) direction. The reservoir is initially filled with saline water, with a density of 1.053g/cm^3 and a viscosity of 1.0 centipoise (cP). We inject CO₂ at a constant rate of 7 Mt/y for 60 years, amounting to a total of 420 million metric tons. During the injection, we assume the supercritical CO₂ to have a density of 776.6g/cm^3 and a viscosity of 0.1cP suggested by (Li et al., 2020) and the Strategic UK CCS Storage Appraisal Project. This two-phase flow simulation provides us with a map of the CO₂ concentration (in percentage) at the aforementioned time steps. We adopt the patchy saturation model (Avseth et al., 2010; Li et al., 2020) to convert these CO₂ concentrations to decreases in bulk moduli and then to decreases in compressional wavespeeds, which are included in Figure 2. From this figure, we can see how the plume develops over time under influence of

buoyancy and the production well to the right. We also observe that the plume gives rise to a difference in p-wavespeed between 50m/s to 300m/s, which should in principle be detectable via seismic monitoring.

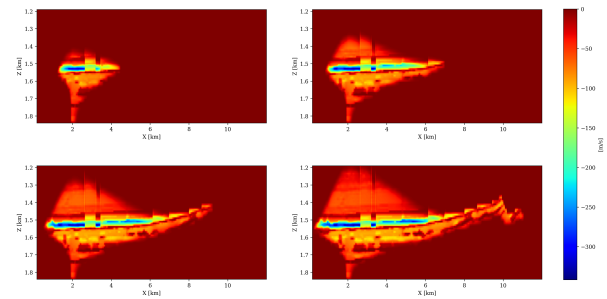


Figure 2: Simulated time-lapse compressional velocity decrease after {15, 30, 45, 60} years of CO₂ injection.

Time-lapse data acquisition

We collect five surveys over a period of 60 years, with a baseline survey conducted before CO₂ injection starts, followed by 4 monitor surveys taken after {15, 30, 45, 60} years of injection. We propose a low-cost sparse non-replicated acquisition scheme with compressive sensing, capable of producing time-lapse seismic data with a high degree of repeatability without relying on replicating the surveys. To keep the costs down, we work with relatively sparsely sampled ocean bottom hydrophones connected to underwater buoys located above the ocean bottom. Compared to ocean bottom nodes, this type of acquisition avoids picking up coherent noise related to interface waves while it shares the advantage of being static and therefore highly replicable. To avoid aliasing, we jitter sample (Herrmann and Hennenfent, 2008) the receiver positions of 64 hydrophones located at a depth of 120m with an average spacing of 250m horizontally. To reduce the costs on the source side, we propose non-replicated continuous simultaneous source shooting, which after deblending (Li et al., 2013; Xuan et al., 2020) yields 1272 sources with a dense source sampling of 12.5m horizontally. To mimic the challenges related to active-source acquisition, we vary for each survey the tow-depth of sources uniformly randomly from 5m to 15m. We also apply random horizontal shifts varying uniformly in a range of -6m to 6m , between sources in the different surveys. Since the receivers are coarsely sampled, we employ source-receiver reciprocity during imaging to further reduce computational costs.

Time-lapse monitoring with the joint recovery model

As stated earlier, we assume to have access to kinematically correct background velocity models $\{\bar{\mathbf{m}}\}_{j=1}^n$. To demonstrate what is in principle achievable under ideal wave-physics, we generate linear data for each vintage via $\delta\mathbf{d}_j = \nabla \mathcal{F}_j(\bar{\mathbf{m}}_j)$, $j = 1 \dots n_v$. We implemented both inversion schemes with [JUDI](#) – the Julia Devito Inversion framework (Witte et al., 2019a). This open-source package uses the highly optimized time-domain finite-difference propagators of [Devito](#) (Luporini et al., 2020; Louboutin et al., 2019). We use a grid spacing of 10m during the wave-equation simulations and a Ricker wavelet with a peak frequency of 25Hz. Despite committing the inversion crime by generating data with the demigration operator, our

monitoring problem is complicated by a rather complex but realistic geology (shown in Figure 1) and by the fact that the sampling is coarse on the receiver site and not replicated at the source site. To increase realism, we also use a random trace estimation technique during imaging. During random trace estimation, memory use is reduced drastically, a prerequisite for scaling our approach to 3D. Using the open-source software [TimeProbeSeismic.jl](#), we chose 32 random probing vectors to approximate our gradient calculations, which leads to noisy imaging artifacts. We refer to Louboutin and Herrmann (2021) and to the proceedings of this conference for further details.

Independent recovery

We first recover the velocity perturbations in each vintage independently. During each Bregman iteration, we randomly select eight shots without replication during imaging, while we select 16 during the first iteration to build up a good starting image. We use the suggested steplength of Lorenz et al. (2014) and the 90th percentile of $|\mathbf{u}_k|$ at the first iteration as the threshold λ . For each vintage, we do 23 Bregman iterations, which amounts to three data passes. To observe the growth of the CO2 plume seismically, we plot the differences of the recovered images for each monitor survey with respect to the baseline in Figure 3. These difference are computed via $\mathbf{x}_j - \mathbf{x}_1$ for $j = 2, \dots, n_v$ where \mathbf{x}_j are the images recovered independently. From these images, we observe that time-lapse signal is visible albeit it is weak while the overall image is plagued by strong artifacts, making it difficult to monitor the CO2 plume.

To quantify the degree of repeatability of the time-lapse images, we follow Kragh and Christie (2002) and use the normalized root mean square (NRMS) values defined as

$$NRMS(\mathbf{x}_1, \mathbf{x}_j) = \frac{200 \times RMS(\mathbf{x}_1 - \mathbf{x}_j)}{RMS(\mathbf{x}_1) + RMS(\mathbf{x}_j)}, \quad j = 2, \dots, n_v. \quad (6)$$

By definition, NRMS values range from 0 to 200 in percentage where a smaller value indicates recovery results are more repeatable, with 10 percent as acceptable by today's best 4D practices. These NRMS values are calculated only using the regions without time-lapse difference.

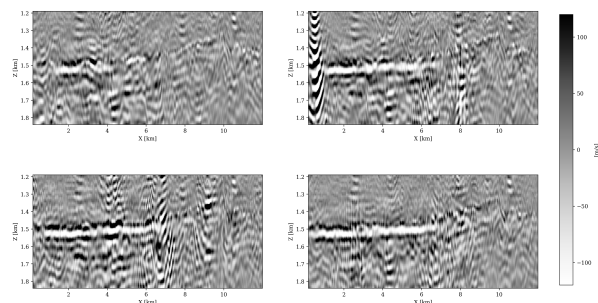


Figure 3: Difference plots w.r.t. the baseline survey yielded by independent recovery. The NRMS values computed for each pair are $\{18.38\%, 15.74\%, 26.63\%, 16.55\%\}$.

Joint recovery

Finally, we recover the common component and innovations jointly via Equation 3 with the same number of data passes (same number of PDE solves) and the same random subsets of

shots as during the independent recovery. For each vintage, a different threshold λ_j is chosen based on the 90th percentile of the corresponding subset of $|\mathbf{u}_k|$ at the first iteration. Figure 4 shows the difference plots. Thanks to the JRM, we observe significantly fewer artifacts except for some artifacts in the middle due to overlapping shots during the early iterations, a problem that can easily be fixed. The improved quality of the difference plots is also reflected in the NRMS values, which are now well within the acceptable range. The scripts to reproduce the experiments in this expanded abstract are made available on the [SLIM GitHub page](#) https://github.com/slimgroup/Software_SEG2021.

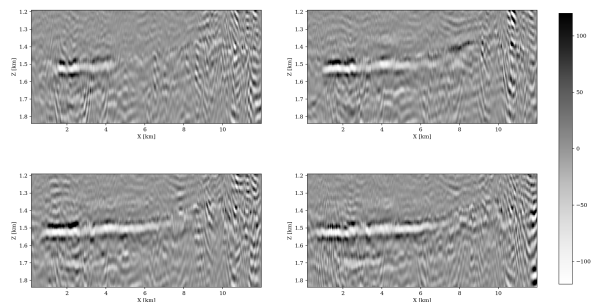


Figure 4: Difference plots w.r.t. the baseline survey yielded by joint recovery. The NRMS values computed for each pair are $\{9.07\%, 8.83\%, 9.62\%, 11.23\%\}$.

DISCUSSION AND CONCLUSIONS

Time-lapse seismic monitoring of carbon storage and sequestration is difficult due to the fact that the velocity changes induced by the growing CO2 plume are relatively small, making it challenging to detect these changes seismically especially when the surveys are poorly sampled and not replicated. By using the joint recovery model, we demonstrably overcome this problem by producing significant improvements in the difference plots associated with a realistic 60 year sequestration scenario. While similar improvements by the joint recovery model have been reported in the literature, the benefit of this approach has not yet been demonstrated for multiple monitor surveys. Neither has this model been used to monitor the development of a CO2 plume in a realistic geological setting in the North Sea that is currently being considered as a site for CO2 sequestration. While these initial results yielding NRMS values of 10% on average are encouraging, many challenges remain in the development of a low-cost 3D seismic monitoring system designed to control and optimize the CO2 sequestration while minimizing its risk.

ACKNOWLEDGEMENT

We would like to thank Charles Jones for the constructive discussion and thank BG Group for providing the Compass model. The CCS project information is taken from the Strategic UK CCS Storage Appraisal Project, funded by DECC, commissioned by the ETI and delivered by Pale Blue Dot Energy, Axis Well Technology and Costain. The information contains copyright information licensed under [ETI Open Licence](#). This research was carried out with the support of Georgia Research Alliance and partners of the ML4Seismic Center.

REFERENCES

- Arts, R., O. Eiken, A. Chadwick, P. Zweigel, L. van der Meer, and B. Zinszner, 2003, Monitoring of cO₂ injected at sleipner using time lapse seismic data, in J. Gale and Y. Kaya, eds., 6th International Conference on Greenhouse Gas Control Technologies: Pergamon, 347–352.
- Avseth, P., T. Mukerji, and G. Mavko, 2010, Quantitative seismic interpretation: Applying rock physics tools to reduce interpretation risk: Cambridge university press.
- Bharadwaj, P., M. Li, and L. Demanet, 2020, SymAE: An autoencoder with embedded physical symmetries for passive time-lapse monitoring: SEG Technical Program, Expanded Abstracts, 1586–1590, doi: <https://doi.org/10.1190/segam2020-3423931.1>.
- Costa, A., 2006, Permeability-porosity relationship: A reexamination of the Kozeny-Carman equation based on a fractal pore-space geometry assumption: Geophysical Research Letters, **33**, L02318, doi: <https://doi.org/10.1029/2005GL025134>.
- Furre, A.-K., O. Eiken, H. Alnes, J. N. Veatne, and A. F. Kier, 2017, 20 years of monitoring cO₂-injection at sleipner: Energy Procedia, **114**, 3916–3926, doi: <https://doi.org/10.1016/j.egypro.2017.03.1523>.
- Herrmann, F. J., 2010, Randomized sampling and sparsity: Getting more information from fewer samples: Geophysics, **75**, no. 6, WB173–WB187, doi: <https://doi.org/10.1190/1.3506147>.
- Herrmann, F. J., and G. Hennenfent, 2008, Non-parametric seismic data recovery with curvelet frames: Geophysical Journal International, **173**, 233–248, doi: <https://doi.org/10.1111/j.1365-246X.2007.03698.x>.
- Janiszewski, F., J. Brewer, and C. Mosher, 2014, Improvements in the efficiency of ocean bottom sensor surveys through the use of multiple independent seismic sources: EAGE Workshop on Land and Ocean Bottom-Broadband Full Azimuth Seismic Surveys, 1–3, doi: <https://doi.org/10.3997/2214-4609.20140388>.
- Kaur, H., A. Sun, Z. Zhong, and S. Fomel, 2020, Time-lapse seismic data inversion for estimating reservoir parameters using deep learning: SEG Technical Program, Expanded Abstracts, 1720–1724, doi: <https://doi.org/10.1190/segam2020-3419749.1>.
- Kragh, E., and P. Christie, 2002, Seismic repeatability, normalized RMS, and predictability: The Leading Edge, **21**, 640–647, doi: <https://doi.org/10.1190/1.1497316>.
- Li, C., C. C. Mosher, L. C. Morley, Y. Ji, and J. D. Brewer, 2013, Joint source deblending and reconstruction for seismic data: SEG Technical Program, Expanded Abstracts, 82–87, doi: <https://doi.org/10.1190/segam2013-0411.1>.
- Li, D., K. Xu, J. M. Harris, and E. Darve, 2020, Coupled time-lapse full-waveform inversion for subsurface flow problems using intrusive automatic differentiation: Water Resources Research, **56**, e2019WR027032, doi: <https://doi.org/10.1029/2019WR027032>.
- Li, X., 2015, A weighted l1-minimization for distributed compressive sensing: PhD thesis, University of British Columbia.
- Li, X., A. Y. Aravkin, T. van Leeuwen, and F. J. Herrmann, 2012, Fast randomized full-waveform inversion with compressive sensing: Geophysics, **77**, no. 3, A13–A17, doi: <https://doi.org/10.1190/geo2011-0410.1>.
- Lorenz, D. A., F. Schopfer, and S. Wenger, 2014, The linearized bregman method via split feasibility problems: Analysis and generalizations: SIAM Journal on Imaging Sciences, **7**, 1237–1262, doi: <https://doi.org/10.1137/130936269>.
- Louboutin, M., and F. J. Herrmann, 2021, Ultra-low memory seismic inversion with randomized trace estimation: ArXiv Preprint ArXiv:2104.00794.
- Louboutin, M., M. Lange, F. Luporini, N. Kukreja, P. A. Witte, F. J. Herrmann, P. Velesko, and G. J. Gorman, 2019, Devito (v3.1.0): An embedded domain-specific language for finite differences and geophysical exploration: Geoscientific Model Development, **12**, 1165–1187, doi: <https://doi.org/10.5194/gmd-12-1165-2019>.
- Lumley, D. E., R. A. Behrens, and Z. Wang, 1997, Assessing the technical risk of a 4D seismic project: SEG Technical Program, Expanded Abstracts, 894–897, doi: <https://doi.org/10.1190/1.1886160>.
- Luporini, F., M. Lange, M. Louboutin, N. Kukreja, J. Huckelheim, C. Yount, P. H. Kelly, F. J. Herrmann, and G. J. Gorman, 2020, Architecture and performance of Devito, a system for automated stencil computation: ACM Transactions on Mathematical Software, **46**, 1–28, doi: <https://doi.org/10.1145/3374916>.
- Maharramov, M., B. Willemsen, P. S. Routh, E. F. Peacock, M. Froneberger, A. P. Robinson, G.W. Bear, and S. K. Lazaratos, 2019, Integrated kinematic time-lapse inversion workflow leveraging full-waveform inversion and machine learning: The Leading Edge, **38**, 943–948, doi: <https://doi.org/10.1190/tle38120943.1>.
- Oghenekohwo, F., and F. J. Herrmann, 2015, Compressive time-lapse seismic data processing using shared information: CSEG annual conference proceedings, Retrieved from <https://slim.gatech.edu/Publications/Public/Conferences/CSEG/2015/oghenekohwo2015CSEGcfl/oghenekohwo2015CSEGcfl.pdf>.
- Oghenekohwo, F., and F. J. Herrmann, 2017, Improved time-lapse data repeatability with randomized sampling and distributed compressive sensing: EAGE Annual Conference Proceedings, doi: <https://doi.org/10.3997/2214-4609.201701389>.
- Oghenekohwo, F., H. Wason, E. Esser, and F. J. Herrmann, 2017, Low-cost time-lapse seismic with distributed compressive sensing-part 1: Exploiting common information among the vintages: Geophysics, **82**, no. 3, P1–P13, doi: <https://doi.org/10.1190/geo2016-0076.1>.
- Qu, X., and D. Verschuur, 2017, Simultaneous joint migration inversion for semicontinuous time-lapse seismic data: SEG Technical Program, Expanded Abstracts, 5808–5813, doi: <https://doi.org/10.1190/segam2017-17778465.1>.
- Queißer, M., and S. C. Singh, 2013, Full waveform inversion in the time lapse mode applied to cO₂ storage at sleipner: Geophysical Prospecting, **61**, 537–555, doi: <https://doi.org/10.1111/j.1365-2478.2012.01072.x>.
- Thomsen, L., 1986, Weak elastic anisotropy: Geophysics, **51**, 1954–1966, doi: <https://doi.org/10.1190/1.1442051>.
- Tian, Y., L. Wei, C. Li, S. Oppert, and G. Hennenfent, 2018, Joint sparsity recovery for noise attenuation: SEG Technical Program, Expanded Abstracts, 4186–4190, doi: <https://doi.org/10.1190/segam2018-2996474.1>.
- Wason, H., F. Oghenekohwo, and F. J. Herrmann, 2015, Compressed sensing in 4-D marine—recovery of dense time-lapse data from subsampled data without repetition: EAGE Annual Conference Proceedings, doi: <https://doi.org/10.3997/2214-4609.201413088>.
- Wason, H., F. Oghenekohwo, and F. J. Herrmann, 2017, Low-cost time-lapse seismic with distributed compressive sensing-part 2: Impact on repeatability: Geophysics, **82**, no. 3, P15–P30, doi: <https://doi.org/10.1190/geo2016-0252.1>.
- Wei, L., Y. Tian, C. Li, S. Oppert, and G. Hennenfent, 2018, Improve 4D seismic interpretability with joint sparsity recovery: SEG Technical Program, Expanded Abstracts, 5338–5342, doi: <https://doi.org/10.1190/segam2018-2975383.1>.
- Witte, P. A., M. Louboutin, N. Kukreja, F. Luporini, M. Lange, G. J. Gorman, and F. J. Herrmann, 2019a, A large-scale framework for symbolic implementations of seismic inversion algorithms in Julia: Geophysics, **84**, no. 3, F57–F71, doi: <https://doi.org/10.1190/geo2018-0174.1>.
- Witte, P. A., M. Louboutin, F. Luporini, G. J. Gorman, and F. J. Herrmann, 2019b, Compressive least-squares migration with on-the-fly fourier transforms: Geophysics, **84**, no. 5, R655–R672, doi: <https://doi.org/10.1190/geo2018-0490.1>.
- Xuan, Y., R. Malik, Z. Zhang, M. Guo, and Y. Huang, 2020, Deblending of OBN ultralong-offset simultaneous source acquisition: SEG Technical Program, Expanded Abstracts, 2764–2768, doi: <https://doi.org/10.1190/segam2020-3428390.1>.
- Yang, D., F. Liu, S. Morton, A. Malcolm, and M. Fehler, 2016, Time-lapse full-waveform inversion with ocean-bottom-cable data: Application on valhall field: Geophysics, **81**, no. 4, R225–R235, doi: <https://doi.org/10.1190/geo2015-0345.1>.
- Yang, D., M. Meadows, P. Inderwiessen, J. Landa, A. Malcolm, and M. Fehler, 2015, Double-difference waveform inversion: Feasibility and robustness study with pressure data: Geophysics, **80**, no. 6, M129–M141, doi: <https://doi.org/10.1190/geo2014-0489.1>.
- Yang, M., Z. Fang, P. A. Witte, and F. J. Herrmann, 2020, Time-domain sparsity promoting least-squares reverse time migration with source estimation: Geophysical Prospecting, **68**, 2697–2711, doi: <https://doi.org/10.1111/1365-2478.13021>.
- Yin, W., S. Osher, D. Goldfarb, and J. Darbon, 2008, Bregman iterative algorithms for l1-minimization with applications to compressed sensing: SIAM Journal on Imaging Sciences, **1**, 143–168, doi: <https://doi.org/10.1137/070703983>.
- Zhang, Z., and L. Huang, 2013, Double-difference elastic-waveform inversion with prior information for time-lapse monitoring: Geophysics, **78**, no. 6, R259–R273, doi: <https://doi.org/10.1190/geo2012-0527.1>.